On-Water Radiometry Measurements: Skylight-Blocked Approach and Data Processing

Zhongping Lee [1], Jianwei Wei [1], Zhehai Shang [1], Rodrigo Garcia [1], Heidi Dierssen [2], Joji Ishizaka [3], Alexandre Castagna [4]

[1] *University of Massachusetts Boston, Boston, Massachusetts 02125, USA*

[2] *University of Connecticut, Connecticut, 06340 USA*

[3] *Institute for Space-Earth Environmental Research, Nagoya University, Japan*

[4] *Protistology and Aquatic Ecology, Gent University, Krijgslaan 281, Gent 9000, BE*

1. INTRODUCTION

The in-water and above-water approaches discussed in Chapters 4 and 5, respectively, <u>derive</u>, rather than directly <u>measure</u>, the water-leaving radiance (L_w). In addition to these 'standard' approaches, there exists a scheme that directly measure L_w for the calculation of remote sensing reflectance (R_{rs}). This scheme attaches an open-ended apparatus (either cone-shaped or cylindrical) to the front of a downward looking radiance radiometer. This apparatus penetrates a few centimeters through the water's surface, while keeping the radiometer in air. This set up effectively blocks surface-reflected light from entering the field-of-view of the radiance radiometer and allows for a <u>direct</u> measurement of L_w. Twenties years ago, Ahn (1999) showed this idea of measuring L_w. Tanaka et al. (2006) tested a dome-cover apparatus to carry out L_w measurements, and Lee et al. (2010) further experimented with a tube that blocked surface-reflected light. More recently, Lee et al. (2013) configured a handy and durable system based on the Satlantic HyperPro II and thoroughly investigated this measurement scheme, which was subsequently termed the skylight-blocked approach (SBA) for the direct measurement of water-leaving radiance. Compared to the standard in-water and above-water approaches, the SBA can be classified as on-water radiometry, but importantly it incorporates an apparatus to block surface-reflected light (Fig. 1). This approach has the following unique features compared to the two standard measurement schemes, whereby:

1) it measures L_w directly; avoiding post-processing procedures such as the extrapolation of $L_u(z)$ to $L_u(0^-)$ required for the in-water approach, or the removal of surface-reflected light required for the above-water approach;

2) it is applicable to any aquatic environment, whereas the in-water approach is challenging to deploy when the bottom depth is shallow and when strong near-surface stratification cause large uncertainties in the extrapolation of $L_u(z)$ to $L_u(0^-)$.

3) it accurately derives the R_{rs} under variable sky conditions, unlike the above-water approach which will generate large uncertainties if there are scattered, moving clouds (even when the Sun is not blocked), or in inland waters (e.g., pond, narrow river or inlet) where diffuse skylight is not easily characterized due to adjacent vegetation or structures.

Similar to in-water radiometry, the SBA measurements are subject to errors due to instrument self-shading. To correct these errors, Shang et al. (2017) developed a correction scheme for processing SBA data based on spectral optimization. The ultimate solution for self-shading effect is to employ an apparatus with a very small diameter (<1 cm for most aquatic environment and for ~350 – 800 nm spectral range). To date, the SBA scheme for L_w (R_{rs}) has been tested in shallow, coastal, and oceanic waters with high performance (Lee et al. 2013; Wei et al. 2015; Wei et al. 2018).

For an accurate determination of the remote sensing reflectance (R_{rs}) robust to environmental conditions, it is important to simultaneously measure both L_w and the downwelling irradiance just above the surface (E_s). This ensures the "same" light environment for both L_w and E_s, and eliminates the restriction imposed by fast changing clouds. Therefore two calibrated radiometers are recommended (as the in-water approach). The final products from SBA generally include spectra of the R_{rs} and the standard deviation (STD). The instrument configuration, measurement and data processing procedures are described as below.
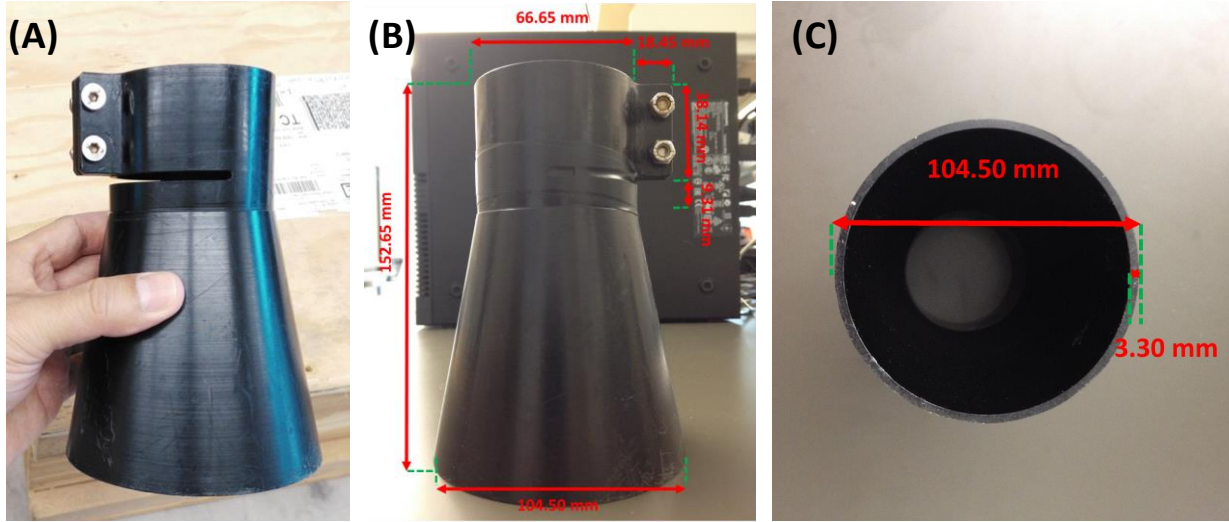

Figure 1. Dimensions of a cone-shaped prototype skylight-blocking apparatus.

2. MEASUREMENTS

Skylight-blocking apparatus

A rule of thumb for the design of the skylight-blocking apparatus is to ensure that it should maximize the measurement performance. First, this apparatus should not be bulky, as self-shading error increases with it's size. Second, it is important to avoid interference with the FOV of the radiometer, as it will add complexity to the radiometric calibration. Third, it should be fabricated in a dark matte color to minimize the light reflection off its own surface. Finally, the apparatus should be weather resistant. An example (see Fig. 1) of such an apparatus was made in the shape of a cone and manufactured from Black Acetron. As illustrated in Figure 1, in this case the cone has a bottom diameter of 104.50 mm, a parallel cross section on the upper side of 66.65 mm in diameter and 105.2 mm in height. The uppermost part of the apparatus is a cylindrical collar attachable to a radiometer. The apparatus shown in Figure 1 was specifically manufactured for commercial radiometers with a FOV of 11.5° in air. For other radiometers with different dimensions and FOV, it is advised to adjust the dimension for the cone or cylinder accordingly. The following formula can be used to calculate the opening of the skylight-blocking apparatus to define its minimum diameter:

$$Y = D + 2 * X * \tan(FOV/2), \tag{1}$$

where X is the distance from the lens to the opening of the skylight-blocking apparatus and D is the effective diameter of the lens.

Instrument configuration

In the deployment, the radiometer with the SBA should be maintained in air such that it receives the light emerging from the water in a specified direction (so far it is commonly in the nadir direction). The base of the cone should be beneath the water surface, while the fore optics of the radiometer located in air. With such viewing geometry, the light

reflected by the sea surface should be blocked by the cone and only the radiance emerging from beneath the water surface will be measured. A configuration for the various components for the L_w measurement is shown in Figure 2. In this example, the radiometer for downwelling irradiance is positioned along with the radiance sensor on a balanced float, so that L_w and E_s are recorded at the "same" location at the "same" time. Other configurations are possible as long as the float is easy to handle, strong enough to hold the sensors, and small enough to minimize impact to the ambient light field.
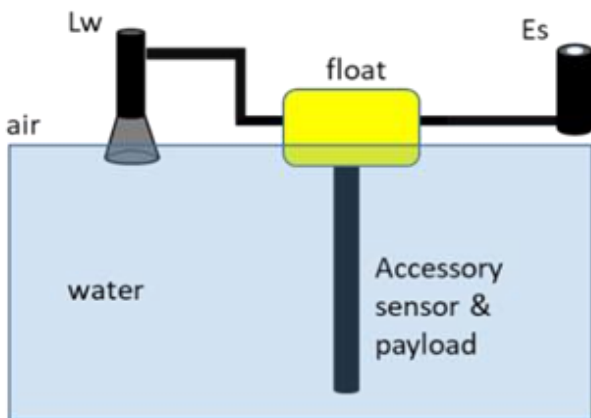

Figure 2. Design and configuration of a prototype radiometric package equipped with SBA. A sonar component for bottom depth is outside of the picture.

Avoidance or minimization of perturbations during deployment

As with in-water and above-water radiometric measurements, perturbations (including those from the float and the upper structure of the ship) to the measurement of L_w and E_s should be avoided or minimized during the deployment of the system. Practically, the instrument package should be kept away from the operating ship to minimize reflection and shadowing from the ship. Based on Monte Carlo simulations, we recommend that a SBA system similar to Figure 2 should be kept at a distance of ~30 m or further in order for ship-induced uncertainty to be less than 1% (Shang, 2019; PhD dissertation). On a slow moving vessel, it is recommended to use caution to avoid white-wash and ship wakes. Specific to the L_w measurements and a configuration similar to Fig. 2, it is strongly recommended that the orientation of the instrument be maintained with the SBA radiance sensor facing the Sun to minimize potential shadowing from the central float. Such an orientation may be achieved by interchanging the two radiance and irradiance radiometers according to the Sun's position, water current and wind directions. For example, if the radiance sensor is faced towards the Sun in the morning, it might be necessary to interchange it with irradiance sensor for similar illumination geometry in the afternoon. To minimize the shadowing effects from the float, an extension arm is recommended to keep the radiance sensor away from the central float. As shown in Figure 2, the arms are about 30 cm in length.

Radiometric calibration

Both radiometers for radiance and irradiance measurements should be calibrated with NIST-traceable standards. Calibration uncertainty of ~1% or less is recommended. The calibration should take into account the stray light correction (SRC), cosine response, polarization sensitivity, etc. (see Chapter 3 of this protocol). As the radiometer fore optics are not expected to be immersed in the water, an immersion factor is not required.

Dark signal

Dark signals should be measured periodically to obtain dark current measurements. This can be done straightforwardly when the radiometers are capable of closing an onboard shutter over the spectrometer before sensor sampling and telemetry output (such as Satlantic's HyperOCR radiometers). Alternatively when no onboard shutters are available, it can also be performed by closing the fore optics with a cap and then taking measurements.

Ancillary data and metadata

Observation time, latitude and longitude coordinates, wind speed, sea state, and instrument tilt are important information for each measurement, although not all will be used for the post-processing of radiometric measurements. Other ancillary information, including water temperature and salinity, are also recommended to facilitate data analysis. For optically shallow waters, it is useful to attach a submersible camera (see Fig. 1) to the float to help identification of benthic composition associated with the reflectance spectra, as well as a sonar component to get the co-registered bottom depth.

Time span for measurements

At each station, a time series (e.g., 5-10 minutes) of continuous measurements of both radiance and irradiance is recorded. This time span usually results in ~500 or more of radiance and irradiance spectra. For field measurement of R_{rs}, there is no intention or assumption that each of these scans is valid. Rather, we will select ~20-50 high-quality spectra for the calculation of final R_{rs} spectrum for the targeted measurement site.

3. DATA ANALYSIS

Data preprocessing

The raw data from both sensors are converted to radiometric units by applying the calibration files and dark current correction. The data are first interpolated onto a common time coordinate. The radiance and irradiance spectra are then interpolated to the same spectral resolution. The instantaneous remote sensing reflectance at time t ($R_{rs}(\lambda, t)$) can be determined from the ratio of the instantaneous $L_w(\lambda,t)$ to the corresponding $E_s(\lambda,t)$:

$$R_{rs}(\lambda,t) = \frac{L_w(\lambda,t)}{E_s(\lambda,t)} \qquad (2)$$

Quality control

To ensure that only high-quality data are collected and used, we check for the instrument tilt and only keep those with low inclination. The need is to avoid apparent Sun zenith cosine changes to the cosine collector of the E_s sensor that can cause large bias. For a system with a single axis inclinometer, only data with tilt ≤ 5° should be used for further analysis (for E_s and nadir-viewing water-leaving radiance). Higher quality can be achieved with a dual axis inclinometer and recording of the system orientation (L_w radiometer facing the Sun). This allows to screen out those measurements with inclinations closer to the Sun's plane (±45°), which may cause up to ±20% E_s bias for tilts >5° across the visible range and for Sun zenith angles between 30° to 60° (Castagna et al. 2019). In the field, prevailing winds, strong currents, waves, white-wash and choppy swell can cause the radiance sensor along with the cone of the SBA system either to pop out of the water surface or to submerge the fore optics of the radiometer into water. As a consequence, raw $L_w(t)$ (and $R_{rs}(t)$) require additional filtering described below:

1) The probability density function (PDF) will be calculated for $R_{rs}(\sim698,t)$ (longer wavelengths are required for optically shallow waters) from the ~500 or more measurements. The first mode of the $R_{rs}(698,t)$ distribution is then located from the PDF.

2) All $R_{rs}(t)$ spectra with $R_{rs}(698,t)$ beyond ±15% of this mode are filtered out.

3) The remaining $R_{rs}(t)$ spectra are considered as the desired high-quality data and used to calculate average and standard-deviation spectra, as in Olszewski and Kowalczuk (2000).

The rational for the above filtering procedure is that

a) for longer wavelengths, water molecules have strong absorption, resulting in very low R_{rs} that may be close to 0, thus an enhancement in the R_{rs} in the longer wavelengths (for oceanic waters and most coastal waters) will likely be the result of surface-reflected light, if the cone swings out of the surface due to swell;

b) "true" R_{rs} of a water body has a specific value, but contributions from surface-reflection or from submersion of the radiance sensor into water are random, so it is this mode reflects "true" R_{rs} of the targeted site.

Self-shade correction

The uncertainty due to self-shading can be quantified with the algorithm of Shang et al. (2017). This algorithm only requires the solar zenith angle (θ_s) and the R_{rs} spectrum obtained in Step 3 listed above (represented as R_{rs}^{Shade} here). The basic workflow of the optimization scheme is referred to the spectral optimization method detailed in Lee et al. (1999). First, an R_{rs} spectrum free of shading error ($R_{rs}^{noshade}$) can be modeled as a function of absorption (a) and backscattering (b_b) coefficients (Gordon et al. 1988; Morel and Gentili 1993):

$$R_{rs}^{noshade}(\lambda) = f_1(a(\lambda), b_b(\lambda)) \,. \tag{3}$$

Further, R_{rs}^{shade} is related to $R_{rs}^{noshade}$ as,

$$R_{rs}^{shade}(\lambda) = R_{rs}^{noshade}(\lambda) * [1 - \varepsilon(\lambda)] \tag{4}$$

where ε is the shading error. Based on Monte Carlo (MC) simulations for the prototype system displayed in Figure 2, ε is a function of a, b_b and θ_s (Shang et al. 2017),

$$\varepsilon(\lambda) = f_2(a(\lambda), b_b(\lambda), \theta_s) \tag{5}$$

Combining with Eq. (3)-(5) yields (size of the cone is omitted):

$$R_{rs}^{shade}(\lambda) = f_3(a(\lambda), b_b(\lambda), \theta_s) \tag{6}$$

Using a spectral optimization procedure, a and b_b can be derived by matching the modeled R_{rs}^{Shade} with the measured R_{rs}^{Shade}. With known θ_s and derived a and b_b, ε can be calculated following Eq. (4). Further, we get:

$$R_{rs}^{true}(\lambda) = \frac{R_{rs}^{Shade}(\lambda)}{1 - \varepsilon(\lambda)} \tag{7}$$

Here, R_{rs}^{true} is the shade-corrected R_{rs} spectrum that is reported for each station. Based on MC simulations, the shading correction algorithm can reduce the measurement errors to $< 2\%$ in the visible domain from oceanic to turbid waters (Shang et al. 2017).

Quality assurance

Quality assurance (QA) should be carried out for each R_{rs} spectrum, and a scheme has been developed to assure the quality of R_{rs} spectra. The QA score system (Wei et al. 2016) is based on the water classification of the R_{rs} spectral shapes. The spectral shape of R_{rs} is represented by the normalized R_{rs} spectrum,

$$nR_{rs}(\lambda_i) = \frac{R_{rs}(\lambda_i)}{\left[\sum_{j=1}^{n} R_{rs}(\lambda_j)^2\right]^{1/2}}, \ i = 1, 2, ..., n \tag{8}$$

where n refers to the number of spectral bands. This system classifies the R_{rs} spectra into predefined optical water types, and then calculate a QA score for each individual R_{rs} spectrum. The QA scores varies from 0 to 1, with 0 referring to the lowest quality and 1 the highest quality. Other methods are also useful including regionally-tuned procedures.

Measurement uncertainty

The measurement uncertainty originates from the environmental disturbances including waves, wave focusing, and data reduction procedure (data filtering, mode determination, shade correction), etc. The total uncertainty from these sources can be evaluated as the standard deviation of the ensemble R_{rs} spectra. Two sample R_{rs} spectra are presented in Figure 3. One spectrum was obtained from the south Yellow Sea and the other measured at the Marine Optical Buoy (MOBY) site, east of Lanai, Hawaii. In general, the standard deviation of such measured R_{rs} spectra is very small.
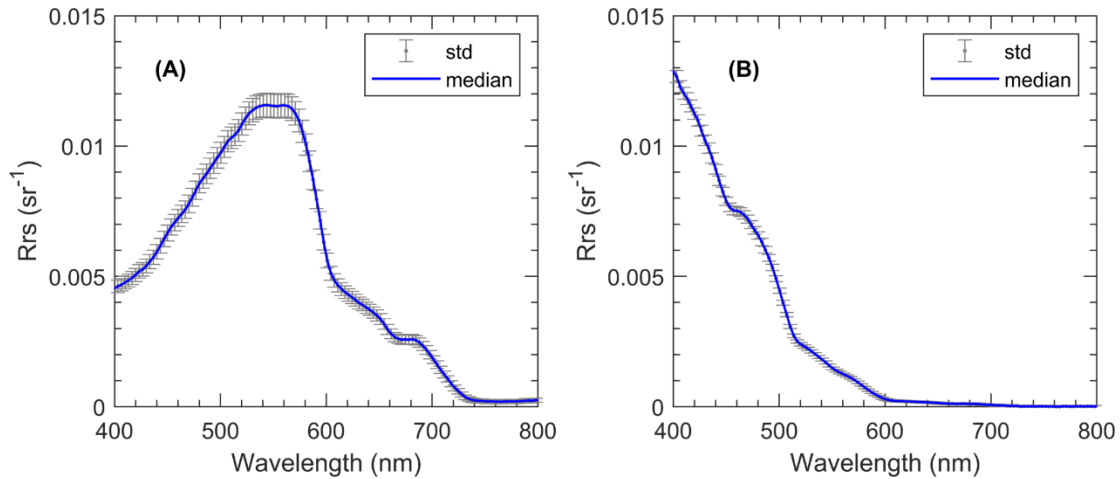

Figure 3. Examples of SBA measured remote sensing reflectance spectra from (a) the South Yellow Sea and (b) the Marine Optical Buoy (MOBY) site.

4. RECOMMENDATIONS AND FUTURE DIRECTIONS

For the configuration given in Figure 2, it is recommend to record meta-data such as the "radiance sensor facing the Sun" or "radiance sensor facing away from the Sun", etc., as it can be informative for assessing the uncertainty due to shading effects. For example, there is likely larger shading impact under high solar zenith angles and if the radiance sensor is oriented away from the Sun. However, this can be avoided or minimized by different configurations, such as placing the radiance radiometer in the middle, rather than on one side of a float. Also, the skylight-blocking apparatus should be customized with respect to the radiometers in use. The critical factors to consider include the radiometer dimensions and sensor's field of view.

The radiometer for E_s can be placed on the operating ship, as long as there is an assurance that the E_s value measured is representative of the E_s value at the location where the radiance radiometer is located. For E_s radiometers positioned similar to that in Figure 2, it is important to keep the cosine collector for E_s above any protrusions on the float system. The largest error source for SBA measurements of water-leaving radiance is self-shading, which is a function of the water's optical properties, sun elevation, and the size of the skylight-blocking cone. Among these three, the cone size is the only parameter that can be determined at the designing/manufacturing phase of this system. Hence, it is highly desired to manufacture small-size radiometers and incorporate a cone as small as possible. In high seas, it is recommended that the integration time of the radiance sensor be short to avoid contamination by surface-reflected light with movement of the cone. Another potential configuration would be to seal the cone and sensor together so that air pressure keeps water from contacting the fore optics.

Separately, Olszewski and Sokolski (1990) proposed a contactless skylight-blocking scheme to screen out surface reflected contributions while taking radiance measurements of water from above the surface. Due to its requirement of both superfast data collection (in ms or less) and very small coverage area (in cm^2 or less) (Olszewski and Sokolski

1990), this scheme has not been widely known or tested. With the advancement of optical-electronic components/systems, it is worth evaluating this above-water SBA and comparing the results from the on-water SBA, as it may provide high-quality R_{rs} while an operation ship is underway.

REFERENCES

Ahn, Y.-H. (1999). Development of redtide & water turbidity algorithms using ocean color satellite. In (p. 287). Seoul, Korea: KORDI

Castagna, A., Johnson, B.C., Voss, K., Dierssen, H.M., Patrick, H., Germer, T.A., Sabbe, K., & Vyverman, W. (2019). Uncertainty in global downwelling plane irradiance estimates from sintered polytetrafluoroethylene plaque radiance measurements., submitted

Gordon, H.R., Brown, O.B., Evans, R.H., Brown, J.W., Smith, R.C., Baker, K.S., & Clark, D.K. (1988). A semianalytic radiance model of ocean color. *J. Geophys. Res., 93*, 10,909-910,924

Lee, Z.-P., Ahn, Y.-H., Mobley, C., & Arnone, R. (2010). Removal of surface-reflected light for the measurement of remote-sensing reflectance from an above-surface platform. *Optics Express, 18*, 26313-26342

Lee, Z.-P., Pahlevan, N., Ahn, Y.-H., Greb, S., & O'Donnell, D. (2013). A robust approach to directly measure water-leaving radiance in the field. *Applied Optics, 52* 1693-1701

Lee, Z.P., Carder, K.L., Mobley, C.D., Steward, R.G., & Patch, J.S. (1999). Hyperspectral remote sensing for shallow waters: 2. Deriving bottom depths and water properties by optimization. *Applied Optics, 38*, 3831-3843

Morel, A., & Gentili, B. (1993). Diffuse reflectance of oceanic waters (2): Bi-directional aspects. *Applied Optics, 32*, 6864-6879

Olszewski, J., & Kowalczek, P. (2000). Sky glint correction in measurements of upward radiance above the sea surface. *Oceanologia, 42*, 251-262

Olszewski, J., & Sokolski, M. (1990). Elimination of the surface background in contactless sea investigations. *Oceanologia, 29*, 213-221

Shang, Z., Lee, Z., Dong, Q., & Wei, J. (2017). Self-shading associated with a skylight-blocked approach system for the measurement of water-leaving radiance and its correction. *Applied Optics, 56*, 7033-7040

Tanaka, A., Sasaki, H., & Ishizaka, J. (2006). Alternative measuring method for water-leaving radiance using a radiance sensor with a domed cover. *Optics Express, 14*, 3099-3105

Wei, J., Lee, Z.-P., & Shang, S. (2016). A system to measure the data quality of spectral remote sensing reflectance of aquatic environments. *J. Geophys. R., 121*, 8189–8207

Wei, J., Lee, Z.P., Garcia, R., Zoffoli, M.L., Armstrong, R., Shang, Z., Sheldon, P., & Chen, R.F. (2018). An assessment of Landsat-8 atmospheric correction schemes and remote sensing reflectance products in coral reefs and coastal turbid waters. *Remote Sensing of Environment, 215*, 18-32

Wei, J., Lee, Z.P., Lewis, M., Pahlevan, N., Ondrusek, M., & Armstrong, R. (2015). Radiance transmittance measured at the ocean surface. *Optics Express, 23*, 11826-11837